Effects of the width of droplet size distribution on soot formation in spray flame

Jun Hayashi[1], Junichi Fukui[1], Noriaki Nakatsuka[1], Fumiteru Akamatsu[1]
[1]Depertment of Mechanical Engineering, Osaka University
Suita, Osaka, Japan

1 Introduction

Spray combustion is a highly complex reactive two-phase phenomenon in which many simultaneous processes affect one another, including dispersion of fuel droplets, their evaporation, chemical reactions of the fuel vapor with the oxidizer, and combustion reaction associated with the formation of soot. Atomization is the earliest process of spray combustion. Spray characteristics, such as mean droplet size, mean spray velocity and droplet size distribution, are determined through the atomization process. Those characteristics have significant effects to the whole processes of spray combustion and spray flame structures [1]. However, since those spray characteristics are difficult to control independently from the other physical characteristics of atomization, effects of the width of droplet size distribution on the spray combustion phenomenon and soot formation in spray flame have not elucidated. In order to clarify the detailed spray flame structures, conducting fundamental experiments and numerical simulations is useful, particularly for simple flow fields such as laminar counterflow. Spray flames stabilized in a laminar counterflow field, in which the reaction zone is well stabilized temporally and spatially, have been accepted as a useful combustion field for investigating their detailed structure [2-12]. The purpose of this study is therefore to investigate the effects of width of droplet size distribution of the fuel spray on the soot formation of spray flames stabilized in a laminar counterflow field. A frequency-tunable vibratory orifice atomizer is employed to carefully control the droplet size distribution [13]. This atomizer is able to generate an arbitrary droplet size distribution independently from the other spray characteristics. Two-dimensional spatial distributions of soot formation area in the spray flames with different droplet size distributions are analyzed by laser induced incandescence (LII). In addition, the detailed local structures of spray combustion characteristics are examined by means of three-dimensional direct numerical simulation (3D-DNS) of spray flames.

2 Experimental Apparatus

Figure 1 shows a schematic illustration of the counterflow burner and stabilized flames in a laminar counterflow field. The upper and lower ports are mounted coaxially and oppositely to one another as shown in Fig.1. Both burner ports are designed to optimize the uniformity of the axial velocity in the radial direction. Liquid fuel is fed into the frequency-tunable vibratory orifice atomizer from a tank pressurized by nitrogen. The atomizer is attached at the top of the upper burner port. The frequency-tunable vibratory orifice atomizer and the typical liquid jet behavior from the atomizer in the case

Correspondence to: j.hayashi@mech.eng.osaka-u.ac.jp

without dispersion air are shown in Fig. 2. The basic mechanism of this atomizer is the same as the one Berglund and Lui had developed [14]. In this study, a pair of piezoelectric ceramic vibrators is attached to the center of the atomizer body and actively vibrates the liquid jet. When the signal frequency changed, the atomization conditions also change within a range of frequencies. As a consequence, the characteristics of spray can be varied without changing other spray characteristics such as the flow rate by controlling the characteristics of implied electric signal [13]. Air flow is supplied into the upper burner port below the atomizer as shown in Fig. 1, and caries the fuel spray downward. Two phase flow of air and n-decane fuel spray are issued to the counterflow field from the upper burner port. A methane/air premixed gas (equivalence ratio ϕ_g = 0.6) flowed into the counterflow field from the lower burner port. This premixed gas is used to form a flat gaseous flame, and the gaseous flame created the stable high temperature region at the proximity of the stagnation plane and simulated a situation in which premixed spray is entering the high temperature region. The gaseous velocities from both ports were kept constant at 0.8 m/s. The strain rate was 53.1 s^{-1}. The flow rate of the fuel spray was kept constant at 0.31 g/min (overall equivalence ratio of liquid fuel ϕ_l = 0.106) under all experimental conditions. These experimental conditions were carefully controlled by float meter. The initial droplet size distribution of the fuel spray was measured at 7 mm below the exit of the upper burner port using a phase Doppler anemometer (PDA, Dantec Electronics Inc.). Typical droplet size distribution of quasi mono- and poly-dispersed droplet size distributions under same Sauter mean diameter (SMD) are shown in Fig. 3. Averaged soot formation characteristics are measured by LII measurement. LII measurement is conducted more than 150 times. A second harmonic Nd:YAG laser (532 nm) was used as the laser source. A laser sheet of 25 mm in width and 0.5 mm in thickness was formed by three cylindrical lenses and irradiated the vertical section, including the center axis. The SMD of the fuel spray is varied from 58 μm to 104 μm.

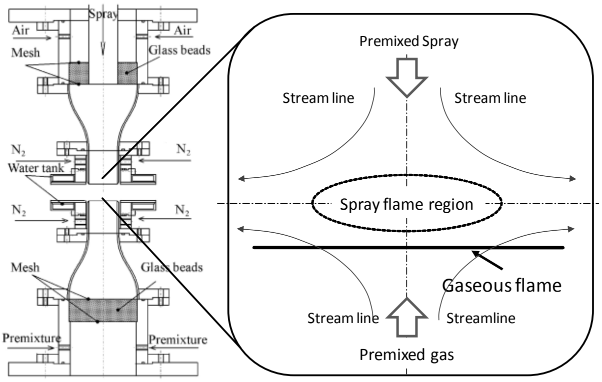

Fig. 1 Schematic illustration of the counterflow burner and stabilized flames in a laminar counterflow field

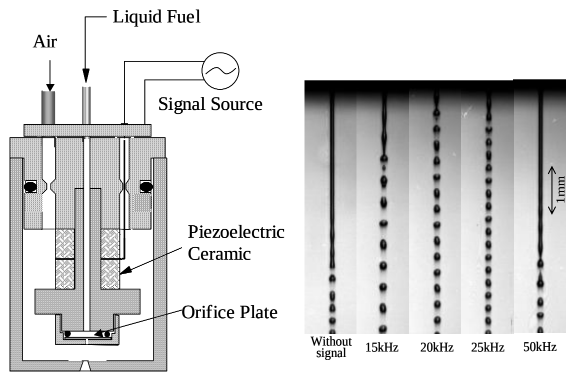

Fig. 2 Frequency-tunable vibratory orifice atomizer and the typical liquid jet behavior from the atomizer in the case without dispersion air

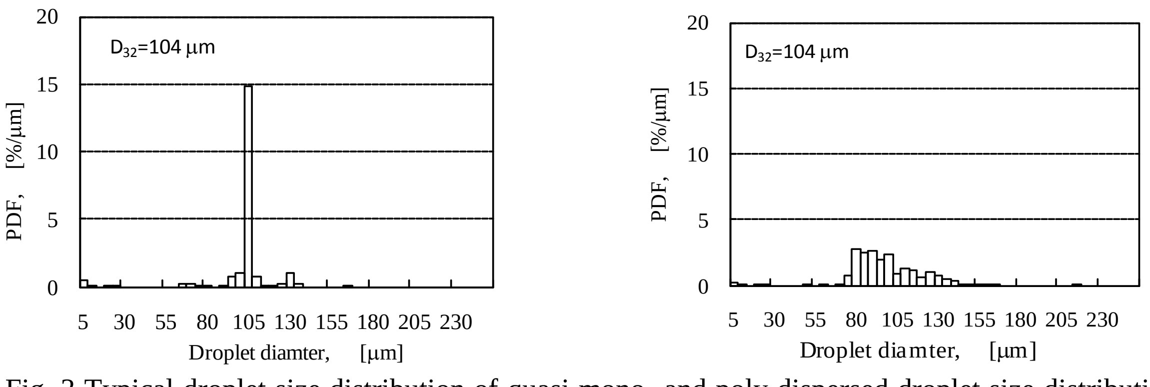

Fig. 3 Typical droplet size distribution of quasi mono- and poly-dispersed droplet size distributions under same Sauter mean diameter and same fuel flow rate (SMD = 104 μm, ϕ_l = 0.106)

3 Formulation and Numerical Simulation Method

A 3D-DNS is applied for spray flames formed in a laminar counterflow field to investigate the effects of width of droplet size distribution in detail. The computational domain for spray flames in a laminar counterflow is designed to match the experimental configuration. The computational domain is shown in Fig. 4. The cylindrical computational domain in the axial and radial directions was 30 mm and 30 mm, respectively. The origin of the computational domain is located at the center of the upper port. For the computation, a 100 × 72 × 100 grid system was used in the radial and circumferential and axial directions. A uniform grid spacing of 0.3 mm was used in the radial and axial directions, respectively. From the upper burner port, Atmospheric air (T = 298 K, P = 0.1013 MPa, volume fraction of nitrogen: 79 % and volume fraction of oxygen volume fraction: 21%) and n-decane spray are issued from 0 mm < r < 21.5 mm of upper burner port. The premixed gas of pre-evaporated n-decane and atmospheric air (T = 298 K, P = 0.1013 MPa, volume fraction of nitrogen: 79 % and volume fraction of oxygen volume fraction: 21 %, equivalence ratio = 0.6) is issued from 0 mm< r < 21.5 mm of lower burner port. From 21.5 mm < r < 23.5 mm) of upper and lower burner port, pure nitrogen is issued as a shield gas. Initial velocities of those gases were 0.8 m/s. Outflow boundary conditions were applied for all quantities on the exit boundary. Two different droplet size distributions under same SMD were calculated (see Fig. 3). Those droplet size distributions of unburned spray were measured experimentally by using PDA. Gaseous phase was calculated in an Eulerian manner, and the governing equations considered for the gaseous phase are mass, momentum, energy, and species mass fraction conservation [15]. Dispersed droplets are randomly injected from the upper port and the values of velocity, temperature and mass of droplets were tracked in a Lagrangian manner. Coupling terms in gas phase equations were treated by PSI-CELL model [16]. In this study, external forces, Soret effect, Dufour effect, pressure gradient diffusion, bulk viscosity, and radiative heat were negrected. For the combustion reaction model, a one-step global reaction for n-decane is adopted. Droplet temperature and mass were calculated by Langumuir-Knudsen evaporation model [17], [18]. The convective terms in governing equations of gaseous phase were discretized by CIP method [19]. Finite difference method and second-order central difference schemes were used to discrete the diffusion terms in governing equations of gas phase. Time integration of all equations are performed via Euler explicit scheme. Thermodynamic and transport properties were calculated with CHEMKIN-II [20] and TRANFIT [21]. The present DNS code for the spray flames has been qualitatively validated in Fukui et al. [22].

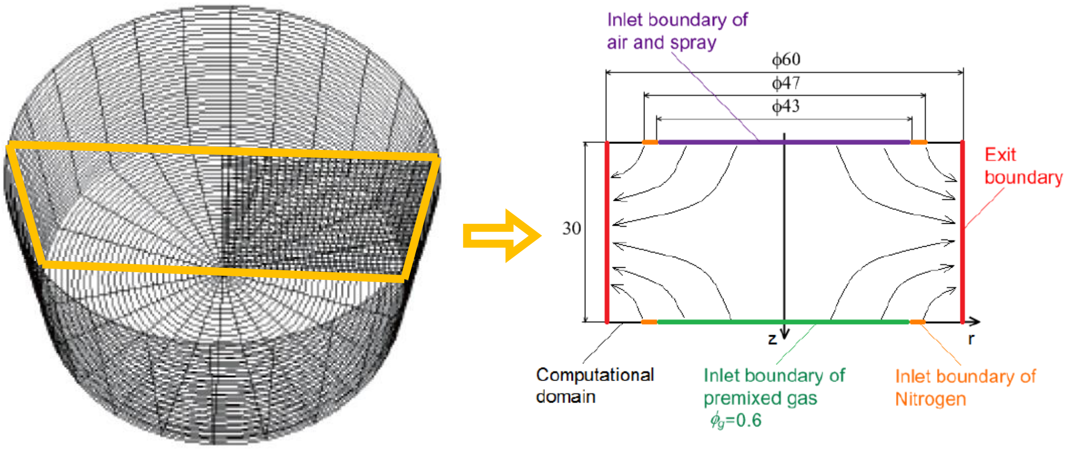

(a) (b)

Fig. 4 Computational domain; (a) overview of computational grid, (b) schematic diagram of computational domain

4 Results and Discussion

Direct photographs (the exposure time = 1/33 s) of formed spray flames in the cases of different droplet size distribution under same SMD condition are shown in Fig. 5. In those direct photographs, Mie-scattering light of the droplets illuminated by laser light of the PDA transmitter, spray flames from the upper burner port, and gaseous flame from the lower burner port are indicated by A, B, and C, respectively. Spray flames form asymmetric because of the temporal and spacial distribution of fuel droplets. Blue and luminous flames are indicated in both photographs. Those flames are considered to correspond to premixed-like and diffusion-like flame, respectively. It is found that the region of diffusion-like flame of poly-dispersed droplet size distribution condition decreased, on the other hand the region of premixed-like flame increased. Since it is well known that the luminosity of diffusion-like flame is including the radiation from soot particles, those changes of flame structures connect to the soot formation. The effect of SMD and droplet size distribution on the ensemble-averaged soot formation area is shown in Fig. 6. The ensemble-averaged values are obtained using 150 LII results. The plots of solid square indicate the soot formation area of the conditions of quasi-mono dispersed droplet size distribution spray, and the plots of void square indicate that the soot formation area of the conditions of poly-dispersed droplet size distribution spray. It is found that the conditions of poly-dispersed droplet size distribution spray have the slightly smaller soot formation area than that of quasi mono-dispersed droplet size distribution spray. These results are thought to be strongly connected with the difference between the spray flame structures of quasi mono- and poly-dispersed droplet size distribution. Here, in order to make poly-dispersed droplet size distribution under same SMD of mono-dispersed droplet size distribution spray, mode droplet size should be decreased. This means that the total evaporation rate decreased with increasing the probability density function of small droplet in spray. As a result, spray flame structures change from diffusion-like flame to premixed-like flame.

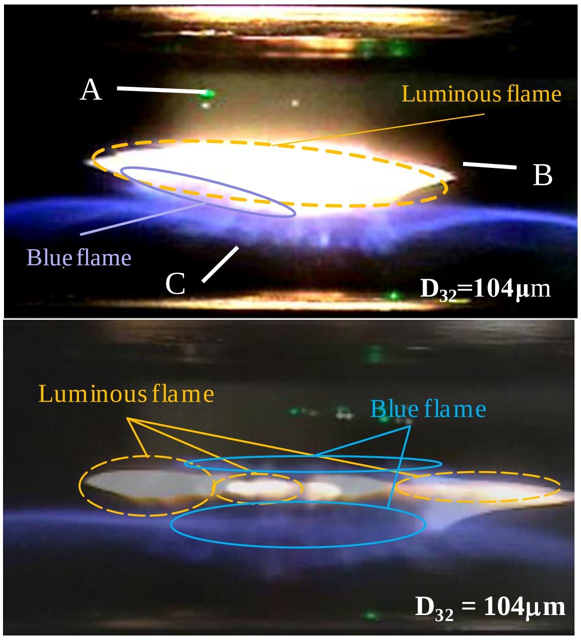

Fig. 5 Direct photographs of formed spray flames in the cases of different droplet size distribution of SMD = 104 μm; (a) quasi mono-dispersed condition, (b) poly-dispersed condition

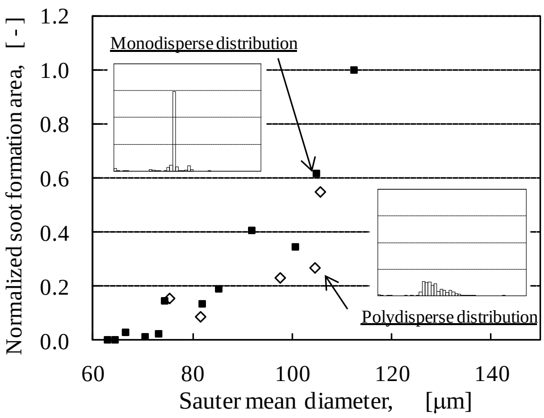

Fig. 6 Effect of SMD and droplet size distribution on the ensemble-averaged soot formation area

These effects of width of droplet size distribution on the spray flame structure and soot formation are also observed by 3D-DNS. Figures 7 show the predicted vertical distributions of time-averaged gaseous temperature and volume fraction of components and flame index of quasi mono- and poly-dispersed droplet size distribution spray under same SMD conditions. It is found that the high temperature region shifts upward. In addition, the volume fraction of fuel vapor at high temperature region is decreased. In order to consider these effects, time-averaged vertical distributions of flame index ($F.I.$) at center is shown in Fig. 7 (b). Here, the $F.I.$ is a parameter to distinguish between premixed and diffusion flames by indicating positive and negative values, respectively, and defined as [23]

$$F.I. = \nabla Y_{C10H22} \cdot \nabla Y_{O2} \tag{1}$$

where Y_{C10H22} and Y_{O2} indicate the mass fractions of n-decane vapor and oxygen, respectively. It can be found that the values of $F.I.$ distribute wider and the positive values are found at the center of negative value under poly-dispersed droplet size distribution condition. This can be considered that the spray combustion area enlarged in axis direction because evaporation rate of poly-dispersed droplet size distribution is varied. Furthermore, a partially premixed-like flame (the positive value of $F.I.$) formed inside of the diffusion-like flame (the negative value of $F.I.$). Those are the reasons why the spray flame of poly-dispersed droplet size distribution condition indicates lower volume fraction at the center of high temperature region.

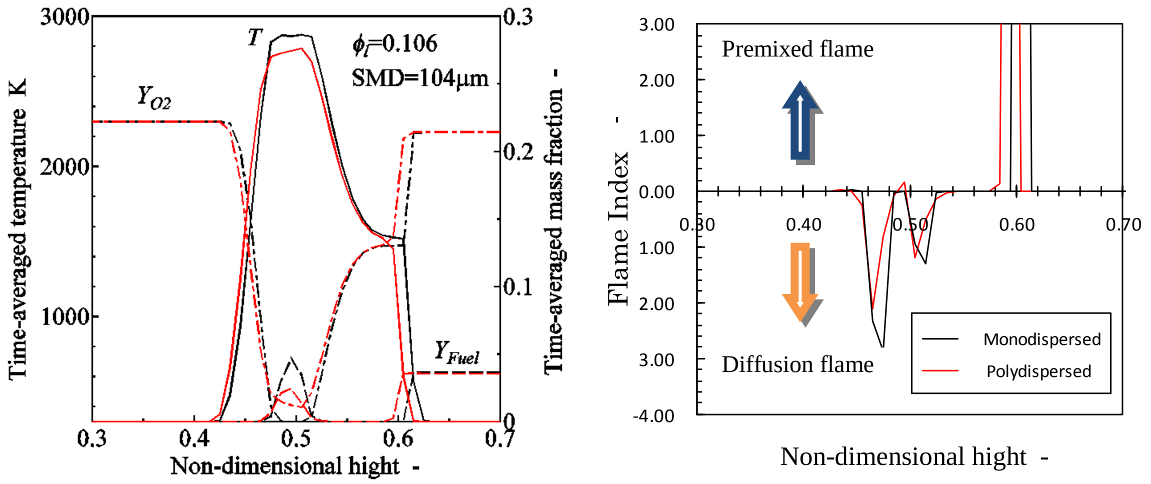

Fig. 7 Predicted vertical distributions of (a) time-averaged gaseous temperature and volume fraction of oxygen and fuel and (b) flame index of poly- and quasi mono-dispersed droplet size distribution spray under same SMD conditions

5 Conclusion

In order to investigate the effects of width of droplet size distribution of the fuel spray on the soot formation of spray flames stabilized in a laminar counterflow. Soot formation characteristics in the spray flames with different droplet size distributions are analyzed by laser induced incandescence (LII). In addition, the detailed local structures of spray combustion characteristics are examined by means of three-dimensional direct numerical simulation (3D-DNS) of spray flames. Results show that the soot formation area decreases in the poly-dispersed droplet size distribution condition. This tendency stems from the difference of flame structure. The portion of premixed-like flame increases under the poly-dispersed droplet size distribution conditions. And the spray combustion area enlarged in axis direction because evaporation rate of poly-dispersed droplet size distribution is varied.

References

[1] A. Williams, Combustion of liquid fuel sprays, (1990), Butterworths.

[2] G. Continillo, W. A. Sirignano, Combustion and Flame 81 (1990) 325-340.

[3] G. Chen, A. Gomez, Proceedings of the Combustion Institute 24 (1992) 1531-1539.

[4] N.-H. Chen, B. Rogg, K. N. C. Bray, Proceedings of the Combustion Institute 24 (1992) 1513-1521.

[5] F. Lacas, N. Darabiha, P. Versaevel, J. C. Rolon, S. Candel, Proceedings of the Combustion Institute 24 (1992) 1523-1529.

[6] S. C. Li, P. A. Libby, F. A. Williams, Proceedings of the Combustion Institute 24 (1992) 1503-1512.

[7] N. Darabiha, F. Lacas, J. C. Rolon, S. Candel, Combustion and Flame 95 (1993) 261-275.

[8] Nakamura, M., Akamatsu, F., Kurose, R. and Katsuki, M., Phys. Fluids 17 (2005) 123301

[9] Mikami, M., Kikuchi, Y., Kojima, N. and Moriue, O., ASPACC2005, (2005) 201-204

[10] Watanabe, H., Kurose, R., Hwang, S.-M. and Akamatsu, F., Combust. Flame, 148 (2007), 234-248.

[11] Watanabe, H., Kurose, R. Komori, S. and Pitsch, H., Combust. Flame, 152(2008), 2-13.

[12] Mikami, M., Mizuta, Y., Tsuchida Y. and Kojima, N., Proceedings of the Combustion Institute, 32 (2009) 2223-2230.

[13] Terashima, K., Shinohara, D., Nakagawa, M., Tokuoka, N., Proceedings of 9th International Conference on Liquid Atomization and Spray Systems, (2003) 3-6.

[14] Berglund, R. N., Liu, B. Y. H., Environmental Science and Technology 7 (1973) 147-153.

[15] Miyauchi, T., Tanahashi, M., Sasaki, K. and Ozaki, T., Transport phenomena in combustion (Chen, C.H., ed.), Taylor and Francis, New York.

[16] Crowe, C.T., Sharma, M.P. and Stock, D.E., Fluids Eng., 99(1977), 325-332.

[17] Miller, R.S., Harstad, K. and Bellan, J., Int. J. Multiphase Flow, 24(1998), 1025-1055.

[18] Miller, R.D. and Bellan, J., J. Fluid Mech., 384(1999), 293.

[19] Yabe, T., Xiao, F. and Utsumi, T., J. Comput. Phys., 169(2001), 556-593.

[20] Kee, R.J., Rupley, F.M. and Miller, J.A., SANDIA Report, SAND89-8009B, (1989).

[21] Kee, R.J., Dixon-Lewis, G., Warnatz, J., Coltrin, M.E. and Miller, J.A., SANDIA Report, SAND86-8246, (1986).

[22] Fukui, J., Hayashi, J. and Akamatsu, F., Proceedings of ICDRES2009, (2009), ID96(CD-R).

[23] Yamashita, H., Shimada, M. and Takeno, T., Proceedings of the Combustion Institute, 26 (1996) 27-34.